Combining Second Harmonic Generation and Multiphoton Excited Photo-Luminescence to investigate TiO2 Nanoparticle Powders

Christian Jonin[1*], Estelle Salmon[2], Faheem Ahmed[3],

Mohammed Benali Kanoun[3], Chawki Awada[3*], and Pierre –Francois Brevet[2]

[1] Laboratoire Charles Coulomb, Université de Montpellier, UMR 5221 CNRS, Montpellier 34095, France.

[2] Institut Lumière Matière, Université de Lyon, UMR 5306 CNRS, Université Claude Bernard Lyon 1, 69622 cedex, Villeurbanne, France

[3] Department of Physics, College of Science, King Faisal University, P.O. Box 400, Al-Ahsa, 31982, Saudi Arabia

- Correspondence: christian.jonin@univ-lyon1.fr ; cawada@kfu.edu.sa.

Abstract : Disentangling Second Harmonic Generation (SHG) and Multiphoton Excited Photoluminescence (MEPL) signals in microscopy experiments is not an easy task. Two methods have been so far proposed based either on a time domain or a spectral domain analysis of the collected signals. In this report, a new method based on polarization discrimination is proposed to separate these SHG and MEPL contributions. In order to demonstrate this operation, intensity depth profiles are recorded for an anatase titanium dioxide powder consisting of 22 nm diameter nanoparticles using ultrafast femtosecond laser excitation. Polarization analysis of these intensity depth profiles is therefore performed and demonstrate a polarization angle shift for the SHG intensity contribution as compared to the MEPL one, allowing for the discrimination of the two SHG and MEPL contributions. The fundamental beam is set at two different wavelengths in order to provide a SHG photon energy above and below the anatase TiO_2 band-gap of 3.2 eV, leading to a change in the relative intensity weight and a spectral shift between the SHG and MEPL contributions. This operation further demonstrates the potential of the method when the spectral domain disentangling cannot be performed. SHG profiles are by far narrower than those of MEPL. This study where both SHG and MEPL contributions are observed offers perspectives in photonics of powder materials as the different origin and properties of the two processes can be separated.

Keywords: TiO_2, Nanoparticles, Powder, Band-gap, Second Harmonic Generation, Multiphoton Excited Photoluminescence, Depth Profiles, Polarization Patterns.

Introduction

Second Harmonic Generation (SHG) is the nonlinear optical process first observed in a quartz plate by Franken et al.[1] by which two photons at a fundamental frequency ω are converted into a single photon at the 2ω harmonic frequency. This phenomenon has been widely used in optical sciences to convert one wavelength into its second harmonic to offer multi-wavelength light sources. Within the electric dipole approximation, this process is forbidden in centrosymmetric media and has therefore been widely used in non centrosymmetric crystals or at interfaces separating two centrosymmetric media[2-3]. Nevertheless, SHG is possible in liquid phases due to the instantaneous molecular orientational fluctuations. Because the process is incoherent in this case, it is also known as Hyper Rayleigh Scattering (HRS).[4] This latter technique has also been used to investigate the nonlinear optical properties of molecules and nanoparticles, plasmonic nanoparticles in particular, dispersed in a liquid solution.[5-6] The SHG process has also been recently used for the study of materials in powder form, material of pharmaceutical interest that do not present a long range non centrosymmetric nature due to their random character.[7] S.K. Kurtz and T.T. Perry pioneered the study of powders by SHG with the objective of determining absolute values of the second-order non-linear susceptibility of materials unavailable as macroscopic crystals.[8] More recently, attention has been given to the SHG intensity resulting from dielectric nano- and micro-powders.[9]

The work presented here focuses on the study of the SHG intensity collected from TiO_2 powders, a material of great interest in the field of photocatalysis or solar energy conversion[10-13]. However, this material presents a rather low band-gap of about 3.2 eV leading therefore to the appearance of a Multiphoton Excited Photo-Luminescence (MEPL) contribution besides the SHG one. Hence, it is compulsory to introduce methods to disentangle the two contributions. In a recent study performed on anatase TiO_2 nanoparticle powders, the

simultaneous appearance of SHG and MEPL has indeed been reported as the fundamental wavelength is tuned over the TiO_2 band-gap.[14] Only MEPL may give rise to a catalytic activity due to the two-photon absorption step whereas SHG does not involve material photo-excitation.[15] Hence discriminating MEPL may prove useful to observe powders during photocatalytic or other chemical processes involving an excitation step whereas SHG may be used as a monitoring method. The present report unfolds therefore two main results. The first one is the separation of incoherent SHG and multiphoton excited photoluminescence (MEPL), including multiphoton excited fluorescence. Here, the use of incoherent SHG due to the nature of powder material precludes a separation from MEPL through some directional selectivity means. Hence, selective directional observation cannot be used as a separation method. It is indeed known that the scattering geometry used to perform SHG experiments is also very well suited to perform MEPL experiments too. Hence, to separate SHG and MEPL contributions, this first result develops a method based on the polarization analysis of the two contributions as opposed to the two other methods, namely the time and the spectral based methods, described previously. The originality of the present work notably lies in the potential use of the method when neither the spectral method, see Ref. 14 for spectral domains where SHG and MEPL cannot be separated, nor the time domain one that may require specific equipment are possible. The second result is the application of the abovementioned polarization based method to separate SHG and MELP contributions in the case of a 22 nm diameter TiO2 powder. Depth profiles are presented where the focus of the fundamental wavelength beam is translated through the air into the powder while the total intensity at the harmonic frequency is recorded. Then, at different fundamental beam focal point positions, polarization resolved intensity patterns were recorded. The subtraction method proposed is shown to be suitable to retrieve the correct narrow-in-depth SHG profile despite the much broader-in-depth MEPL profile. It has to be noted that besides powders, this method can be

applied to molecular compounds dispersed in a solid host matrix or in solution. Note here that multiple scattering is the main origin of the intensity decrease as the focus is translated into the powder material whereas for molecular compounds immersed in a matrix, the latter decrease may rather originate from absorption. Separating SHG and MEPL has also importance due to the possible presence of a coherent contribution besides the incoherent one due to the interface where the centrosymmetric may be broken. The disentangling of the two phenomena is thus here applied on the TiO_2 system where MEPL and SHG, by their intrinsic nature, may reveal different properties, like photocatalysis and structural changes for instance.

Experimental setup

The present study has been performed using the SHG experimental set-up described in details in the previous study on the TiO_2 powder by Jonin et al..[14] Briefly, a femtosecond Ti: sapphire laser (Coherent, model Mira 900) with a fundamental wavelength in the 770 – 790 nm range and a repetition rate of 76 MHz with pulse duration of about 180 femtoseconds was used at an average energy per pulse of about 0.5 nJ. It has to be noted that the Laser Induced Damage Threshold is about 0.6 $J.cm^{-2}$.[16] The linear polarization angle of the fundamental input beam was selected with a half-wave plate and a red filter was placed afterwards to remove any second harmonic light generated prior to the sample. The fundamental beam was focused onto the anatase TiO_2 powder by a X16 microscope objective with a numerical aperture of 0.32 providing a spot size of (5.0+/-0.5) microns in diameter. This microscope objective was placed on a vertical motorized translation stage (Thorlabs, model KMTS50E) to move the focal point from air to the air/powder interface and then into the bulk of the powder. The SHG and the MEPL signals generated from the sample were collected in retro-reflection. A dichroic mirror was placed above the objective to separate the signal generated from the fundamental one. A polarizing cube coupled to a half wave-plate was placed along the

harmonic path allowing the selection of the output polarization. The polarized harmonic beam was then focused by a 25 mm focal length lens onto the entrance slit of the spectrometer (Spex, model 500 M) and then collected by a cooled CCD camera (Andor, model DU 440). The experiment was controlled with a custom-written LabVIEW software.

Material and methods

In the present work, the study was performed on an anatase TiO_2 powder formed from 22 nm diameter nanoparticles synthesized using the sol-gel method which is described in details by Faheem et al..[17] The size of the TiO2 powder nanoparticles was about 22 nm in diameter, on average, Raman spectrum and SEM image are provided in Figs. S3 and S4 in Supplementary File as further characterizations. Experimentally, the powder was placed on a glass substrate and gently compressed with another glass plate to obtain a rather flat air/powder interface. This second plate was then removed to provide an air/powder interface. Vertical profiles of the SHG and MEPL intensities were then obtained by moving the vertical position of the fundamental beam focus from the air into the powder with a depth step of 2 µm, see Figure 1. The MEPL depth profile exhibited peaks which were not further studied but likely arising from the random character of the powder. Figure 2 displays spectra collected for fundamental wavelengths of 772 nm and 788 nm in retro-reflection for the focal point where the SHG intensity is at its maximum at the air-powder interface. This vertical position was defined as the reference position z = 0.

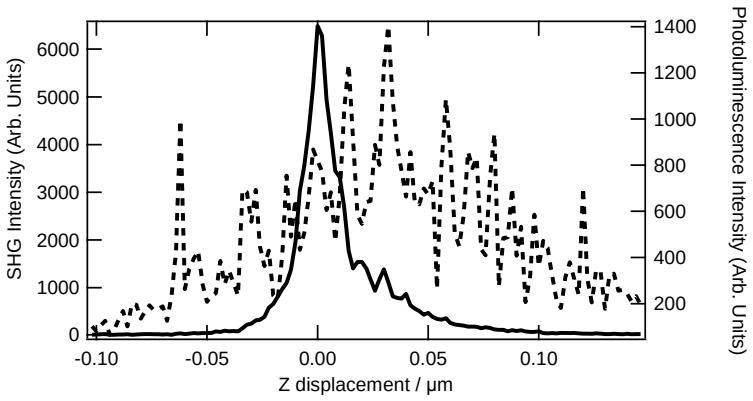

Figure 1 : Intensity depth profiles recorded at 772 nm for (full line) SHG and (dashed line) MEPL.

Hence, for a selected fundamental wavelength, and by tuning the fundamental beam focal point z position, intensity depth profiles were obtained for the SHG and the MEPL processes. As seen from Figure 2(a), the two SHG and MEPL processes are clearly observed and can be well separated spectrally by a careful choice of the fundamental beam wavelength. Indeed, for the 772 nm fundamental wavelength, the SHG line is located at 386 nm, easily identified by the simple law of the fundamental wavelength divided by two. The second band corresponding to the MEPL contribution is rather broad spanning the 400 – 430 nm range and exhibits a maximum at around 405 nm. In this configuration, the SHG line is clearly separated from the MEPL band and the spectral method is well suited to perform an individual analysis of the SHG and MEPL contributions. However, at the fundamental wavelength of 788 nm, see Figure 2(b), the spectrum exhibits a clear superposition of the SHG and MEPL intensities. Considering the spectra reported in Figure 2(a)-(b) for two different incident fundamental wavelengths, intensity depth profiles can thus be recorded separately for the SHG and the MEPL contributions with a careful choice of the spectral range of integration of the collected intensity. A 10 nm spectral integration width was assumed for the SHG band whereas a 30 nm spectral integration width was selected for the MEPL, well separated from the range where

the SHG signal is expected, i.e. away from the fundamental wavelength divided by two. As it is shown below, the different width of the spectral range of integration is not an impediment for the analysis and can be renormalized afterwards for further analysis.

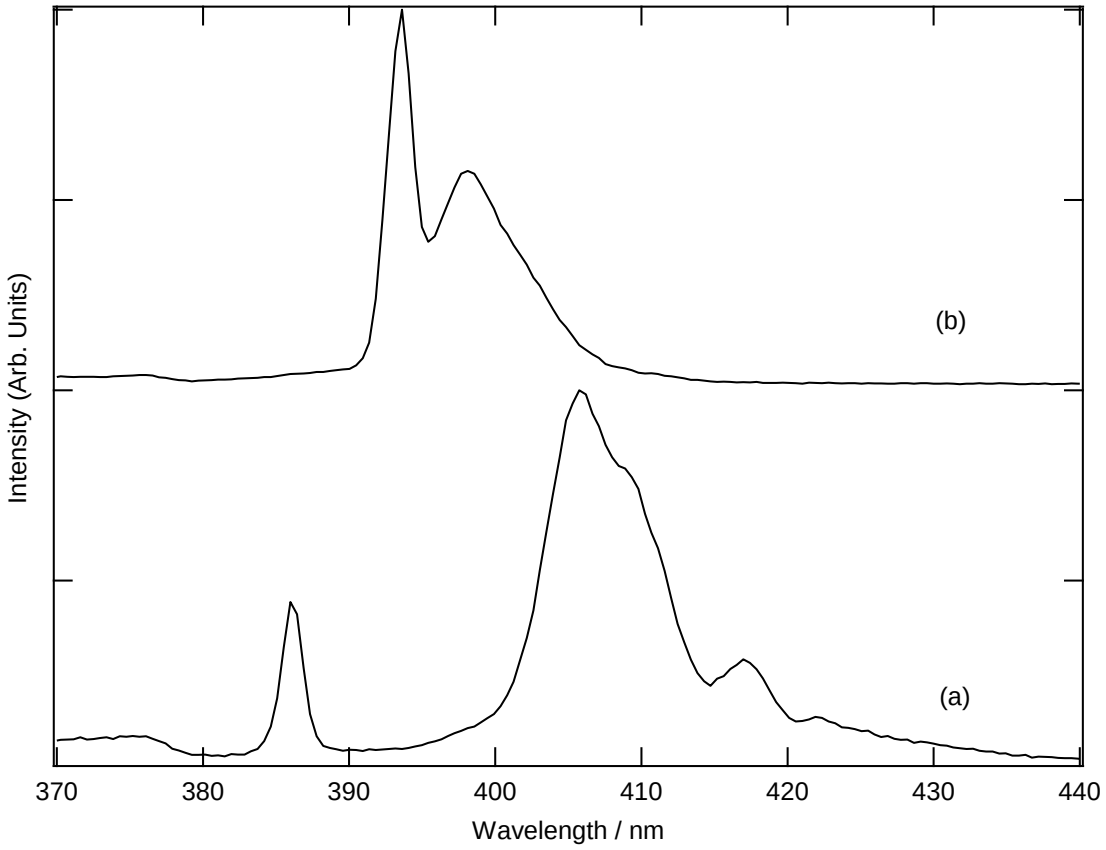

Figure 2: SHG and MEPL spectra recorded for the fundamental beam focal point located at z = 0. The incident fundamental wavelength is fixed at (a) 772 nm and (b) 788 nm.

The SHG intensity depth profile exhibits a typical un-symmetric behavior, with a sharp rise on the negative depths side, i.e. when the fundamental beam focal point is still in the air, and a slower decrease on the positive depths, i.e. when it is entering the bulk of the powder, see Figure 1. This behavior is similar to that reported by Sanchez- Dena *et al* for the $LiNbO_3$ powders.[18] Depth profiles result from the combination of the squared longitudinal intensity profile of the translated focused fundamental TEM00 Gaussian beam on the rising edge and

an exponential-like decay on the decreasing edge at positive depths due to the simultaneous extinction stemming from multiple scattering and re-absorption when photon energies are above band gap. It has to be noted that both SHG and MEPL can be observed simultaneously because they are spectrally separated when the fundamental wavelength is 772 nm. At a fundamental wavelength of 788 nm, only MEPL can be observed separately by choosing the wavelength range of integration outside the SHG line. Around 394 nm, SHG and MEPL are superposed and cannot be separated easily. One objective of the present study is to discriminate these two contributions in this condition.

An elegant solution to this problem of separating the MEPL contribution from the SHG one has been proposed in the time domain based on the difference between time-dependent MEPL characterized by its time decay and instantaneous SHG scattered light known as SHG.[19-21] Typical values for MEPL or fluorescence lifetimes are of the order of nanoseconds or longer whereas the characteristic time for SHG is given by the fundamental laser pulse length. With the use of a temporal gating combined with fast counting electronics, easy discrimination can be achieved between MEPL and SHG photons. A second method to perform this separation is to use the spectral properties as the SHG wavelength can be shifted through the tuning of the fundamental wavelength whereas MEPL cannot due to its origin associated to the material resonance properties. This latter method may not be used in all circumstances. Indeed, if it is not possible to spectrally shift the SHG response sufficiently far out of the MEPL domain, this separation cannot be performed. In the present study, we thus propose a third method to discriminate between SHG and MEPL contributions based on their distinctive polarization response.[22] This method is achieved with the recording of polarization resolved intensity graphs as the fundamental beam input polarization is rotated for a fixed output polarization.

The corresponding polarization resolved graphs for the present TiO_2 powder study are displayed in Figure 3.

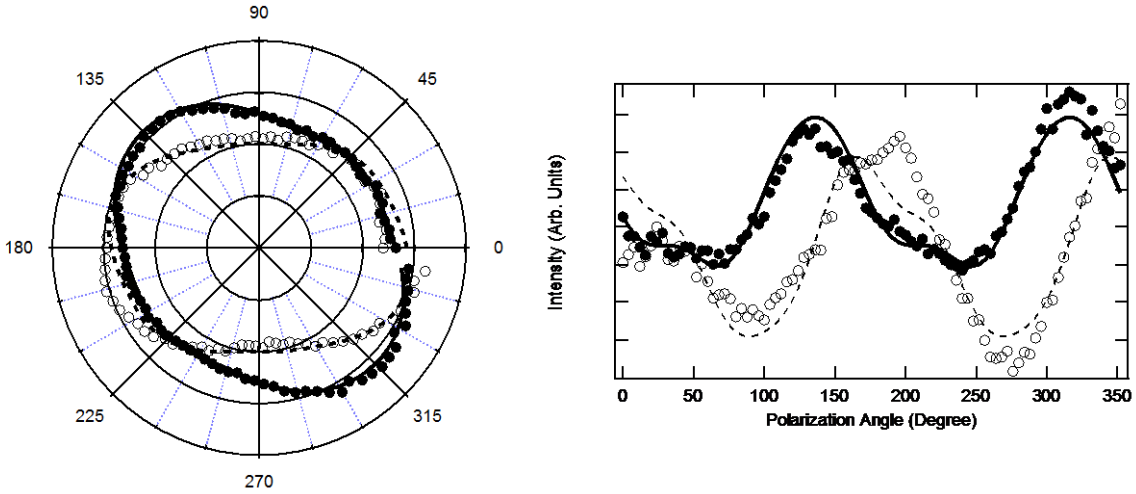

(a) (b)

Figure 3 : (a) Polar plot Polarization resolved intensity graphs recorded at z = 0 depth position for (filled circles) the SHG line and (empty circles) the MEPL band. The SHG and MEPL curve fits are in solid and dashed lines, respectively. The fundamental wavelength is fixed at 772 nm. (b) Same plot rescaled to emphasize the polarization shifts.

Both SHG and MEPL polarization intensity graphs exhibit a largely polarization insensitive pattern indicative of the dominating random medium emission as noted above but still possess a distinctive polarization dependence, see Figure 3(a)-(b). A clear polarization angle shift between the two graphs is therefore observed, with that of the SHG line exhibiting a secondary weaker contribution identical to that of the MEPL, see Figure 3(b). This observation is in agreement with the spectral analysis performed in Figure 2 for the fundamental wavelength of 772 nm and exhibiting at the SHG wavelength a superposition of the SHG contribution with a minor MEPL one.

In order to provide quantified parameters for SHG and MEPL polarization resolved graphs, the SHG intensity collected was modeled according to the standard theory already presented elsewhere and extended here for MEPL.[18] In particular, the polarized SHG intensity as a function of the fundamental beam polarization angle γ writes as :

$$I_{SHG}^{\gamma} = a_5 + \sum_{i=0}^{4} a_i \cos^i(\gamma - \gamma_{SHG}) \sin^{4-i}(\gamma - \gamma_{SHG}) \quad (1)$$

with intensity coefficients a_i and a polarization shift γ_{SHG}. In particular, the sum over the *i* index must be taken from zero up to four because of the quadratic dependence of the SHG field with the fundamental beam amplitude. Odd powers of the sine and cosine functions remain because there are no intensity time fluctuations as opposed to the case of liquid solutions for example. However, for MEPL, because the latter phenomenon stems from the next order of the power expansion of the nonlinear polarization with the field amplitude, the latter sum must be taken from zero up to six, namely :

$$I_{MEPL}^{\gamma} = b_7 + \sum_{i=0}^{6} b_i \cos^i(\gamma - \gamma_{MEPL}) \sin^{6-i}(\gamma - \gamma_{MEPL}) \quad (2)$$

Finally, the total intensity collected follows :

$$I_{Total}^{\gamma} = I_{MEPL}^{\gamma} + I_{SHG}^{\gamma} = I_{SHG}^{\gamma}(1 + \alpha) \quad (3)$$

with the $\alpha = I^{\gamma}_{MEPL}/I^{\gamma}_{SHG}$ parameter scaling the relative weight of the MEPL contribution with respect to that of SHG. Adjustment of the polarization plots with the above three equations are also presented on Figure 3 and the different resulting fitting parameters are reported in Table S1. Note that the adjustment procedure entailed first the adjustment of the MEPL alone by selecting the adequate spectral domain and then of the combined SHG and MEPL contributions maintaining fixed the parameters obtained for MEPL alone. As expected, in the case of the two SHG and MEPL contributions collected at 772 nm excitation well separated in Figure 2, no MEPL contribution remains and the adjusted α value is close to zero. The same study was performed again at the fundamental excitation wavelength of 788 nm where the MEPL contribution largely overwhelms that of SHG. The SHG intensity depth profile obtained at this 788 nm fundamental wavelength using the spectral method is displayed in Figure 4. Again, the SHG intensity depth profile is used to define the z depth reference to perform the polarization study. The polarization analysis was repeated at four different depths and the value of the $\alpha(z)$ parameter then extracted. The polarization graphs are reported in the Supplementary Information file as Figures S1(a)-(c) except for the z = 0 position for which the polar graphs are presented in Figure 5.

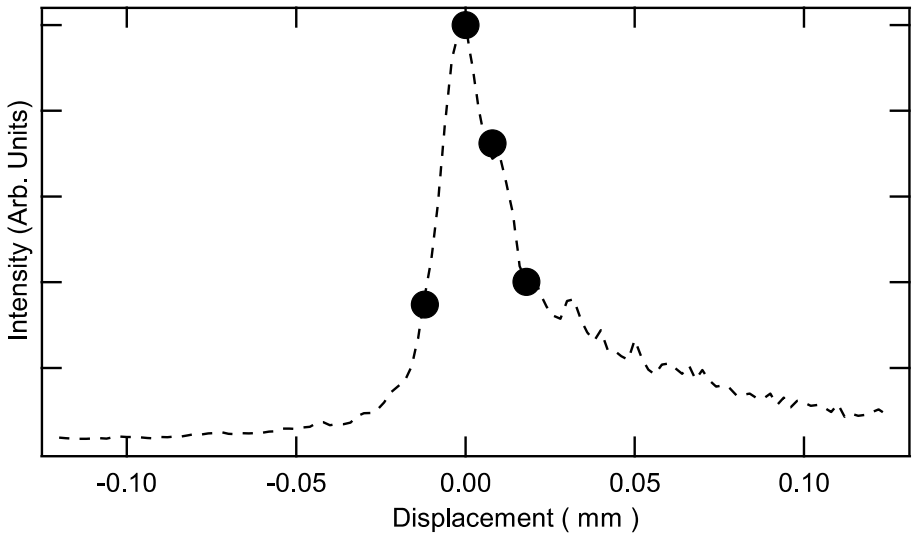

Figure 4 : Intensity depth profile recorded at 788 nm. The filled disks indicate where the polar measurements were performed.

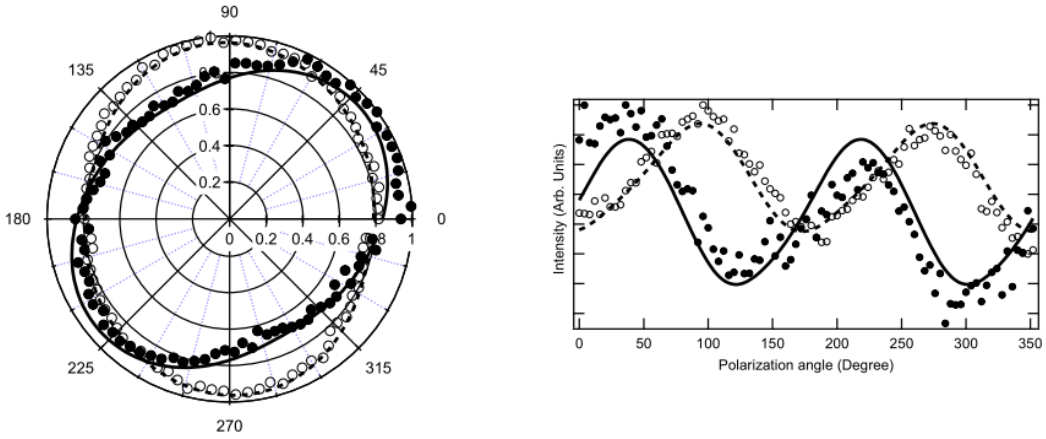

(a) (b)

Figure 5 : (a) Polarization resolved intensity graphs recorded at z = 0 depth position for (filled circles) the SHG line and (empty circles) the MEPL band. The SHG and MEPL curve fits are in solid and dashed lines, respectively. The fundamental wavelength is fixed at 788 nm. (b) Same plot rescaled to emphasize the polarization shifts.

The corresponding adjustment parameters are given in Table S2. At this fundamental excitation wavelength of 788 nm, the weight of the MEPL contribution, as given by the $\alpha(z)$ parameter, dominates over that of SHG, as confirmed with the spectral analysis given in Figure 2(b), see Table S3. The dependence of the unit-less $\alpha(z)$ parameter with the depth position of the beam focus and extracted from the polar measurements is displayed in Figure S2. The values of the $\alpha(z)$ parameter are provided for $\gamma = 0$.

In order to adjust the depth dependence of the $\alpha(z)$ parameter, the model previously developed by Sanchez-Dena *et al.* was used and adapted to MEPL as well.[18] It reads as follows, where the $\alpha(z)$ parameter is indeed a function of depth, namely :

$$\alpha(z) = G\frac{\int_{-\infty}^{+\infty}\left|\frac{\exp(-\epsilon_{MEPL}z)}{\sigma_{MEPL}^2+(z\prime-z)^2}\right|^3 dz\prime}{\int_{-\infty}^{+\infty}\left|\frac{\exp(-\epsilon_{SHG}z)}{\sigma_{SHG}^2+(z\prime-z)^2}\right|^2 dz\prime} \quad (4)$$

where G is a general constant and the SHG and MEPL contributions convolutions of a Lorentzian profile of width σ with an exponential decrease of characteristic parameter ϵ. Considering the total intensity collected as the mere superposition of the SHG and the MEPL contributions, since the two contributions do not present mutual coherence, the MEPL contribution can be suppressed and the SHG contribution depth profile recovered. In order to perform an assessment of the method, Figure 6 displays the SHG depth profile obtained using the spectral method, the depth profile displaying both SHG and MEPL contributions and finally the SHG depth profile where the MEPL contribution is suppressed using the polarization method described above. It is pointed out that this operation is possible because it has been controlled that the MEPL polarization pattern is identical over the whole MEPL band.

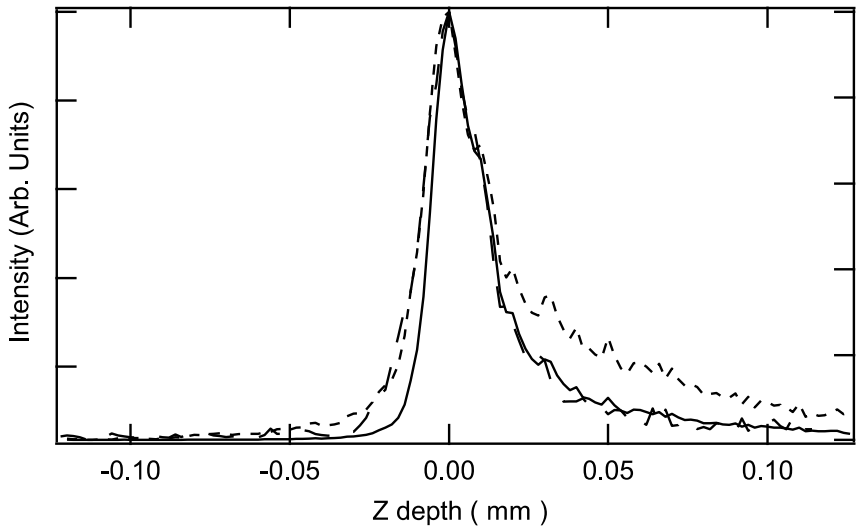

Figure 6 : Depth profiles recorded at 788 nm fundamental wavelength excitation for (dashed) intensity combining both SHG and MEPL contributions, (long dashed) intensity of the SHG contribution with MEPL contribution suppressed using the spectral method, (full) intensity of the SHG contribution with MEPL contribution suppressed using the polarization method.

Both the spectral method and the newly proposed polarization method lead to narrower intensity depth profiles once the MEPL is suppressed. This feature underlines the differences into the two processes. Despite MEPL being of higher order as compared to SHG, MEPL being of third order as compared to SHG that is of second order only in the nonlinearity, MEPL appears with a broader depth profile, possibly due to the symmetry constraints. Indeed, SHG is forbidden in centrosymmeric materials like anatase TiO_2 whereas MEPL is not. This feature nevertheless provides a way to investigate random materials generating simultaneously SHG and MEPL. Separation of the two SHG and MEPL contributions can be achieved with three different methods, namely temporal, spectral or polarization methods, and therefore should pave the way to use one phenomenon to monitor the material as the second one is used to photo-induce a reaction. This would be expected in the case in photo-catalysis

for example where SHG is used to monitor the system whereas MEPL is used to initiate the reaction.

Conclusions

It is therefore shown in this work that it is possible to separate the SHG and MEPL contributions collected from a random nano-powder using a polarization analysis where both the spectral and the time domain analysis would not be suitable. It is interesting to emphasize here that the random character of this material introduces a further degree of complexity due to the weak dependence of the total intensity collected with the fundamental exciting beam polarization angle. Hence, the method will be even more efficient for a medium that does not introduce depolarization of the collected light, underlining its robustness. Obviously, perfect random media will likely provide perfectly unpolarized light precluding the use of this analysis. This method constitutes a third approach to separate SHG and MEPL intensity contributions besides the spectral and temporal methods and is thus applicable to a wide range of materials, for instance powders of different grain size or liquid solutions of dyes. Of course, the SHG and MEPL polarization characteristics must differ to be separated.

This new method based on the polarization analysis constitutes with the time and spectral domain methods a set of three methods to separate SHG and MEPL contributions because, as opposed to SHG that does not involve medium excitation, MEPL does. Therefore, MEPL can further initiate chemical reactivity upon material light absorption whereas SHG constitutes a simultaneous analytical tool witnessing the undergoing phenomena. This disentangling operation is therefore crucial in the understanding of nonlinear excitation of materials.

Acknowledgments:

The authors extend their appreciation to the Deputyship for Research & Innovation, Ministry of Education in Saudi Arabia for funding this research work through the project number 1063.

References

(1) P.A. Franken, A.E. Hill, C.W. Peters, G. Weinreich, Generation of Optical Harmonics, Phys. Rev. Lett., 1961, 7, 118.

(2) Y.R. Shen, The Principles of Nonlinear Optics, Wiley, New York, 1984.

(3) P.F. Brevet, Surface Second Harmonic Generation, Presses Polytechniques Universitaires Romandes (PPUR), Lausanne, 1997.

(4) R.W. Terhune, P.D. Maker, C.M. Savage, Measurements of Nonlinear Light Scattering, Phys. Rev. Lett., 1965, 14, 681.

(5) K. Clays, A. Persoons, Hyper Rayleigh Scattering in Solution, Phys. Rev. Lett., 1991, 66, 2980.

(6) J. Nappa, G. Revillod, I. Russier-Antoine, E. Benichou, C. Jonin, P. F. Brevet, Electric Dipole Origin of the Second Harmonic Generation of Small Metallic Particles, Phys. Rev. B, 2005, 71, 165407.

(7) A.U. Chowdhury, S. Zhang, G.J. Simpson, Powders Analysis by Second Harmonic Generation Microscopy, Anal. Chem., 2016, 88, 3853.

(8) S.K. Kurtz, T.T. Perry, A Powder Technique for the Evaluation of Nonlinear Optical Materials, J. Appl. Phys., 1968**,** 39, 3798.

(9) O. Sanchez-Dena, E.V. García-Ramírez, C.D. Fierro-Ruíz, E. Vigueras-Santiago, R. Farías, J.A. Reyes-Esqueda, Effect of Size and Composition on the Second

Harmonic Generation from Lithium Niobate Powders at Different Excitation Wavelengths, Mater. Res. Express, 2017, 4, 35022.

(10) A. Fujishima, K. Honda, Electrochemical Evidence for the Mechanism of the Primary Stage of Photosynthesis, Bull. Chem. Soc. Japan, 1971, 44, 1148.

(11) L. Lin, Z. Jiang, C. Zhu, X. Hu, X. Zhang, H. Zhu, J. Fan, Enhanced Optical Absorption and Photocatalytic Activity of Anatase TiO2 through (Si,Ni) Co-doping, Appl. Phys. Lett., 2012, 101, 62106.

(12) W.J. Yin, H. Tang, S.H. Wei, M.M. Al-Jassim, J. Turner, Y. Yan, Band Structure Engineering of Semiconductors for Enhanced Photoelectrochemical Water Splitting: The Case of TiO2, Phys. Rev. B, 2010, 82, 45106.

(13) L. Liu, Y. Jiang, H. Zhao, J. Chen, J. Cheng, K. Yang, Y. Li, Engineering Coexposed (001) and (101) Facets in Oxygen-Deficient TiO2 Nanocrystals for Enhanced CO2 Photoreduction under Visible Light. ACS Catal., 2016, 6, 1097.

(14) C. Jonin, E. Salmon, Z. Behel, F. Ahmed, M. Benali Kanoun, C. Awada,, P.F. Brevet, Simultaneous Second Harmonic Generation and Multiphoton Excited Photoluminescence in Anatase TiO2 Nanopowder, Opt. Materials, 2022, 132, 112857.

(15) R.W. Boyd, Nonlinear Optics, Academic Press, New York, 2008.

(16) J. Yao, Z. Fan, Y. Jin, Y. Zhao, H. He and J.Shao, Investigations of damage threshold to TiO2 coatings at different laser wavelength and pulse duration, Thin. Solid. Films, 2008, 516, 1237.

(17) A. Faheem, M. B. Kanoun, C. Awada, Ch. Jonin, P.F. Brevet, An Experimental and Theoretical Study on the Effect of Silver Nanoparticles Concentration on the Structural, Morphological, Optical and Electronic Properties of TiO2 Nanocrystals, Crystals, 2021, 11, 1488.

(18) O. Sanchez-Dena, Z. Behel, E. Salmon, E. Benichou, J.A. Reyes-Esqueda, P.F. Brevet, Ch. Jonin, Polarization-Resolved Second Harmonic Generation from LiNbO3 Powders, Opt. Mat., 2020, 107, 110169.

(19) O. F. J. Noordman, N. F. van Hulst, Time-Resolved Hyper-Rayleigh Scattering: Measuring First Hyperpolarizabilities β of Fluorescent Molecules, Chem. Phys. Lett. 1996, 253, 145.

(20) G. Olbrechts, K. Wostyn, K. Clays, A. Persoons, High-frequency Demodulation of Multiphoton Fluorescence in Long-Wavelength Hyper-Rayleigh Scattering, Opt. Lett., 1999, 24, 403.

(21) K. Wostyn, K. Binnemans, K. Clays, A. Persoons, Hyper-Rayleigh Scattering in the Fourier Domain for Higher Precision: Correcting for Multiphoton Fluorescence with Demodulation and Phase Data, Rev. Sci. Instrum., 2001, 72, 3215.

(22) P. Němec, F. Pásztor, M. Brajer, I. Němec, Spectrally- and Polarization-Resolved Hyper-Rayleigh Scattering Measurements with Polarization-Insensitive Detection, Optics Commun., 2017, 388, 21.

Supplement Information File

Combining Multiphoton Excited Photoluminescence and Second Harmonic Generation to investigate TiO2 Nanoparticle Powders.

Christian Jonin[1*], Estelle Salmon[2], Faheem Ahmed[3],

Mohammed Benali Kanoun[3], Chawki Awada[3], and Pierre –Francois Brevet[2]

1 Polarization Resolved Intensity Plots of SHG and MEPL at 788 nm excitation wavelength

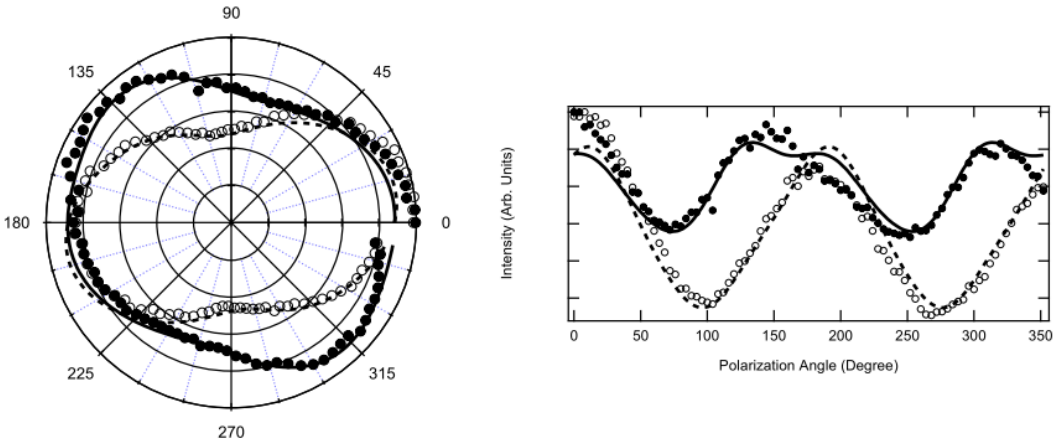

Figure S1a : Polar graphs of the SHG (full circles) band and the MEPL (empty circles) contributions. The SHG and MEPL curve fits are in solid and dashed lines, respectively. The depth position is z = - 0.012 mm

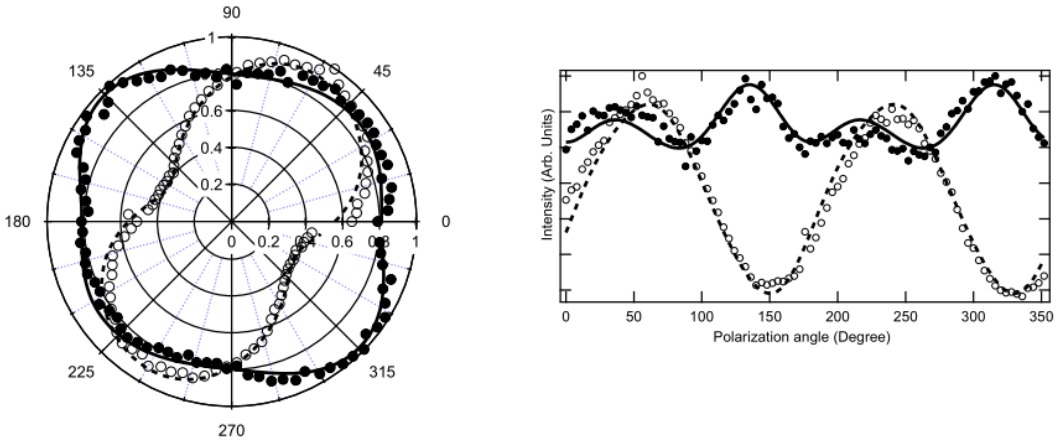

Figure S1b : Polar graphs of the SHG (full circles) band and the MEPL (empty circles) contributions. The SHG and MEPL curve fits are in solid and dashed lines, respectively. The depth position is z = 0.008 mm

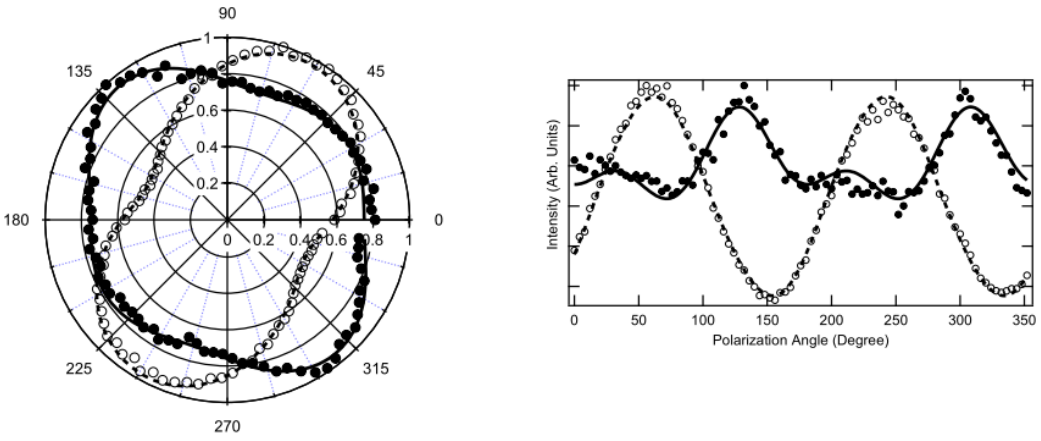

Figure S1c : Polar graphs of the SHG (full circles) band and the MEPL (empty circles) contributions. The SHG and MEPL curve fits are in solid and dashed lines, respectively. The depth position is z = 0.012 mm

2 Depth dependance of the $\alpha(z)$ parameter

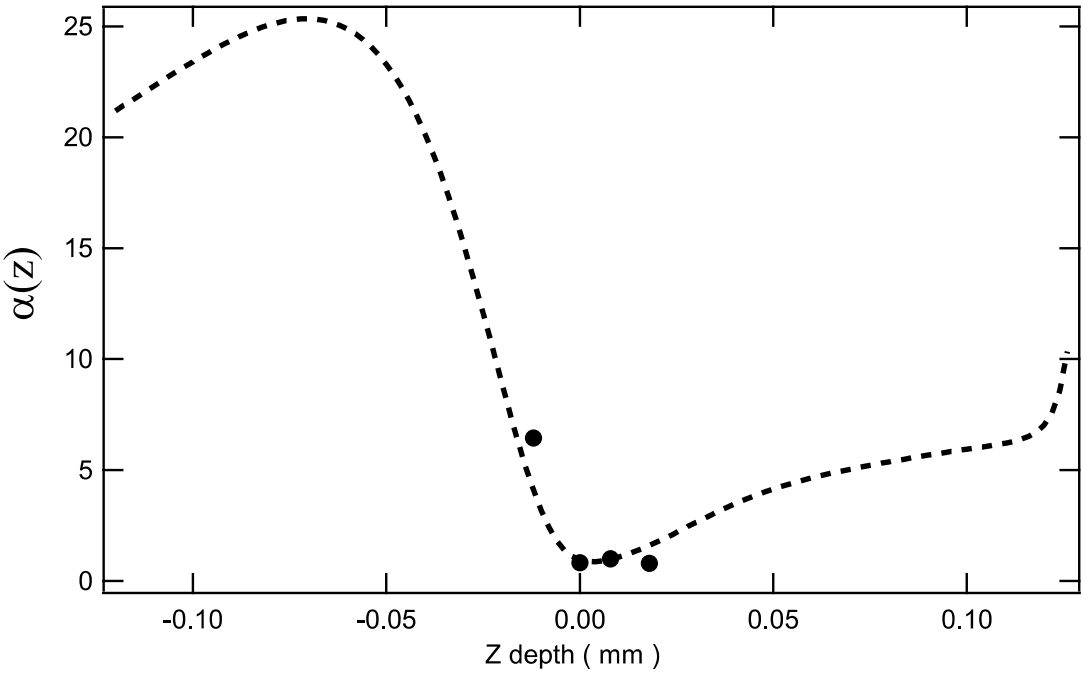

Figure S2 : Depth dependence of the α(z) parameter determined from the polar graphs fitted with Eqs.(1)-(3). Dashed line is an adjustment using Eq.(4).

3 Adjustment Parameters of the SHG and MEPL contributions at 772 and 788 nm excitation wavelength

Table S1 : Parameters of the adjustment procedure of the polarization graph given in Figure 3 using Eqs.(1)-(3) and recorded at a fundamental wavelength of 772 nm.

Fit Parameters	$z = 0$
a_0	0.15±0.05
a_1	-0.01±0.01
a_2	-0.25±0.05
a_3	-0.27±0.03

a_4	-0.15±0.05
a_5	0.22±0.08
γ_{SHG}	6.78±0.10
b_0	0.02±0.01
b_1	0.02±0.01
b_2	0.33±0.07
b_3	0.31±0.08
b_4	0.70±0.10
b_5	-0.18±0.02
b_6	0.29±0.01
b_7	0.60±0.10
γ_{MEPL}	-2 .80±0.10

Table S2 : Parameters of the adjustment procedure of the polarization graphs given in Figure 5 and Figure S1 using Eqs.(1)-(3) and recorded at a fundamental wavelength of 788 nm for different z depth positions in mm.

Fit Parameters	$z = -0.012$	$z = 0$	$z = 0.008$	$z = 0.018$
a_0	-0.14±0.06	0.17±0.03	0.03±0.07	0.08±0.02
a_1	-0.09±0.01	0.40±0.10	-0.42±0.08	-0.40±0.10
a_2	-0.26±0.04	0.53±0.07	0.59±0.01	0.64±0.06
a_3	-0.34±0.06	0.50±0.10	-0.86±0.04	-1.32±0.08
a_4	-0.14±0.06	0.18±0.02	0.02±0.08	0.08±0.02
a_5	0.40±0.10	0.62±0.08	0.41±0.09	0.53±0.07

γ_{SHG}	8.32±0.08	2.09±0.01	9.22±0.08	3.74±0.06
b_0	-0.08±0.02	0.42±0.08	0.20±0.10	0.23±0.07
b_1	0.20±0.10	-0.03±0.07	0.48±0.02	0.46±0.04
b_2	0.14±0.06	0.75±0.05	0.42±0.08	0.54±0.06
b_3	0.23±0.07	-0.03±0.07	0.85±0.05	0.81±0.09
b_4	0.57±0.03	0.59±0.01	0.07±0.03	0.29±0.01
b_5	0.30±0.10	0.04±0.06	0.55±0.05	0.46±0.04
b_6	0.28±0.02	0.14±0.06	0.01±0.09	0.02±0.01
b_7	0.57±0.03	0.64±0.06	0.57±0.03	0.59±0.01
γ_{MEPL}	-6 .25±0.05	-0.78±0.02	2.07±0.03	4.20±0.10

4 Numerical values for the depth dependance of the $\alpha(z)$ parameter

Table S3 : $\alpha(z)$ parameter value provided for $\gamma = 0$ and at for the different depth.

Z depth in mm	-0.012	0	0.008	0.018
$\alpha(z)$	6.44±0.60	0.82±0.08	1.00±0.10	0.79±0.08

5 Anatase TiO_2 powder

Scanning Electron micrograph (SEM) picture of the TiO2 nanoparticle powder sample.

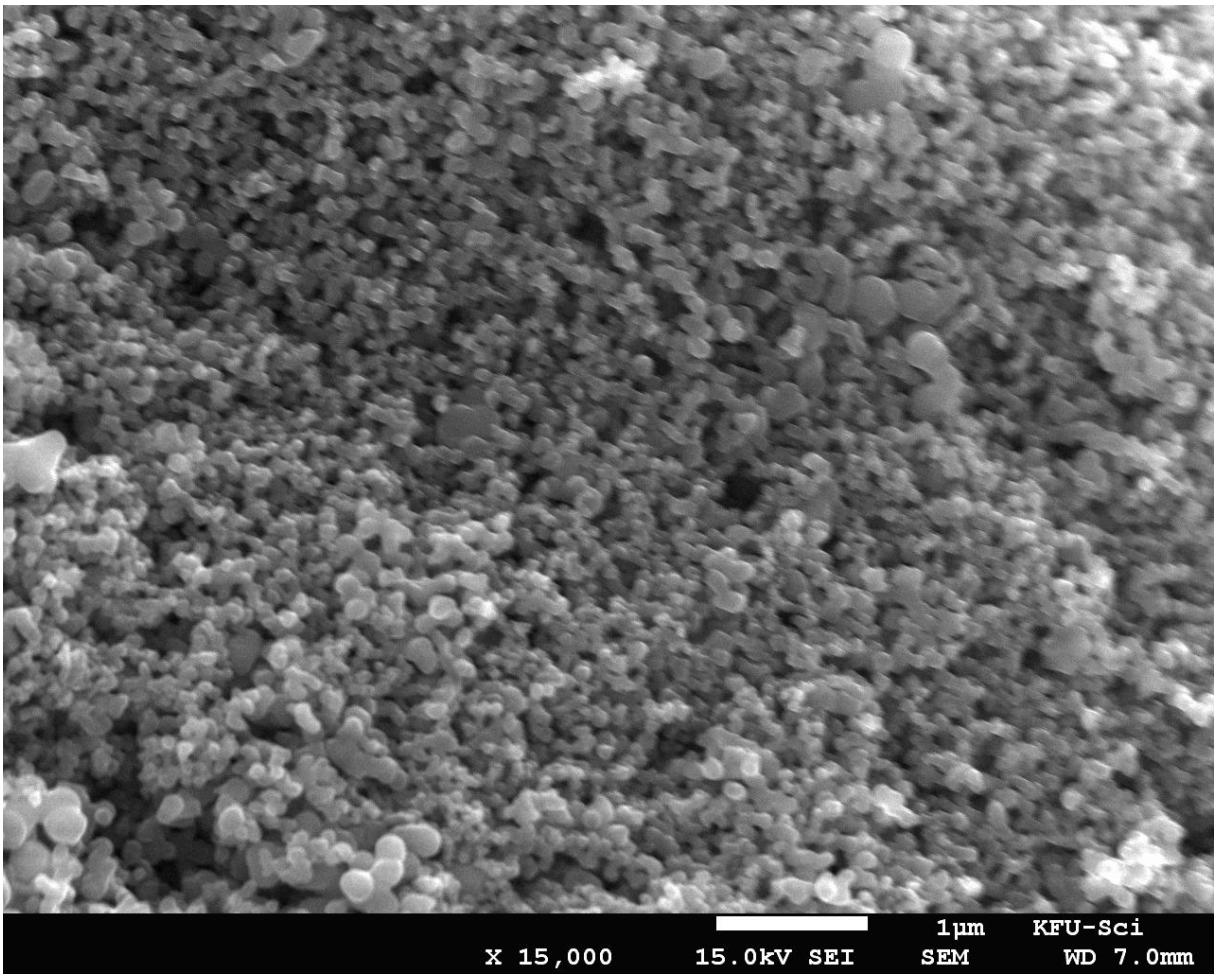

Figure S3 : Scanning Electron Micrograph (SEM) image of the anatase TiO_2 powder sample.

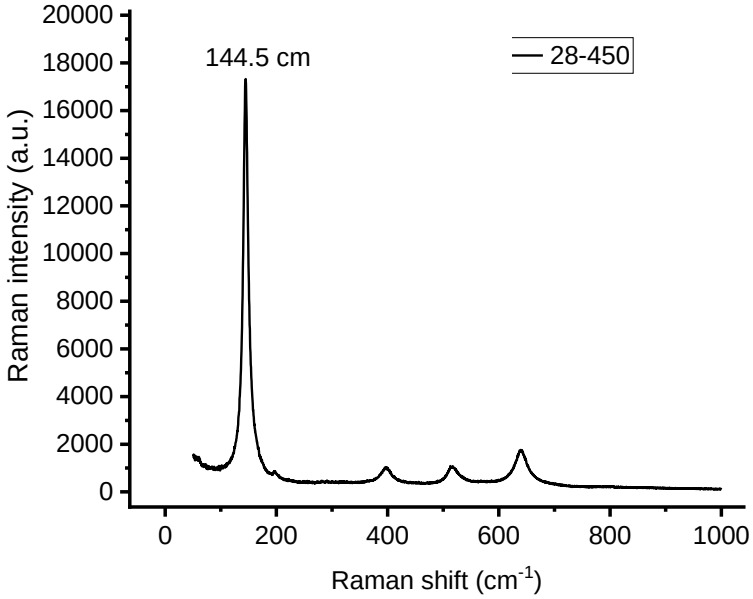

Figure S4 : Raman spectra of pure TiO_2 nanoparticles. An intense Raman peak at 145 cm^{-1} is observed, which can be assigned to the Eg optical Raman mode of anatase TiO_2. The other Raman peaks at 196 cm^{-1},394 cm^{-1}, 512 cm^{-1}, and 636 cm^{-1} were assigned to E_g, B_{1g}, A_{1g}, and E_g Raman modes of anatase TiO_2, respectively.

6 Schematics of the experimental setup

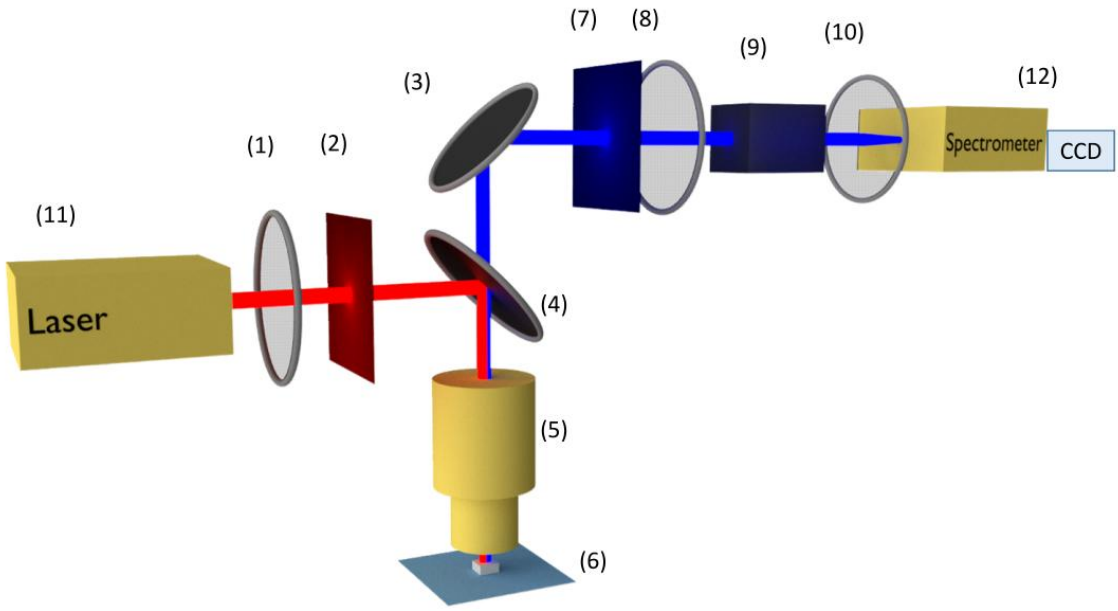

Figure S5 : Schematics of the Experimental setup : (1) Half waveplate (2) Low pass filter (3) mirror (4) Dichroic Mirror (5)Microscope Objective (6) sample (7) High pass filter (8) Half waveplate (9) polarizing Cube (10) Lense (11) Ti:Sa femtosecond laser (12) Detection system.